Available online at www.sciencedirect.com

ScienceDirect

Physics Letters B 654 (2007) 58–64

PHYSICS LETTERS B

www.elsevier.com/locate/physletb

# Direction-sensitive dark matter search results in a surface laboratory

Kentaro Miuchi [a,*], Kaori Hattori [a], Shigeto Kabuki [a], Hidetoshi Kubo [a], Shunsuke Kurosawa [a], Hironobu Nishimura [a], Yoko Okada [a], Atsushi Takada [a], Toru Tanimori [a], Ken'ichi Tsuchiya [a], Kazuki Ueno [a], Hiroyuki Sekiya [b], Atsushi Takeda [b]

[a] *Cosmic-Ray Group, Department of Physics, Graduate School of Science, Kyoto University Kitashirakawa-oiwakecho, Sakyo-ku, Kyoto 606-8502, Japan*
[b] *Kamioka Observatory, ICRR, The University of Tokyo Higashi-Mozumi, Kamioka cho, Hida 506-1205, Japan*

Received 19 February 2007; received in revised form 11 June 2007; accepted 16 August 2007

Available online 29 August 2007

Editor: H. Weerts

**Abstract**

We developed a three-dimensional gaseous tracking device and performed a direction-sensitive dark matter search in a surface laboratory. By using 150 Torr carbon-tetrafluoride ($CF_4$) gas, we obtained a sky map drawn with the recoil directions of the carbon and fluorine nuclei, and set the first limit on the spin-dependent WIMP (Weakly Interacting Massive Particles)-proton cross section by a direction-sensitive method. Thus, we showed that a WIMP-search experiment with a gaseous tracking device can actually set limits. Furthermore, we demonstrated that this method will potentially play a certain role in revealing the nature of dark matter when a low-background large-volume detector is developed.


*PACS:* 14.80.Ly; 29.40.Cs; 29.40.Gx; 95.35.+d

*Keywords:* Time projection chamber; Micro pattern detector; Dark matter; WIMP; Direction-sensitive

## 1. Introduction

Revealing the nature of dark matter has received much more attention since the successive results of the WMAP cosmic microwave background all-sky observation [1]. Many dark matter direct search experiments have been concluded [2–7], are currently being performed [8–14], or are in the planning stage [15]. Weakly interacting massive particles (WIMPs) are very plausible candidates of dark matter. Most dark matter search experiments are designed to measure only the energy transferred to the nucleus through WIMP-nucleus scatterings. In these experiments, the distinct signals of WIMPs are the annual modulation of the energy spectrum. Because the amplitude of an annual modulation signal is only a few % of the rate, positive signatures of WIMPs are very difficult to detect with these detectors [4]. On the other hand, the motion of the solar system with respect to the galactic halo is considered to provide a much larger asymmetry in the direction-distribution of the WIMP velocity observed at Earth [16]. A detection method of a positive signature of WIMPs by measuring the directions of the nuclear recoils have been studied [2,6,14,17]. If the distribution of the local halo were not isotropic—perhaps quite clumpy—direction-sensitive methods would then potentially provide information on it.

Gaseous detectors are one of the most appropriate devices to detect this "WIMP-wind" [18,19]. The DRIFT project has performed underground measurements for more than two years with 1 $m^3$ time projection chambers (TPC) filled with a low-pressure $CS_2$ gas aiming to detect the mainly WIMP-wind via spin-independent (SI) interactions [14]. Since former studies suggest to perform the WIMP-search both via SI and spin-dependent (SD) interactions [20,21], we proposed a SD-sensitive WIMP-wind search, named NEWAGE (New generation WIMP-search with an Advanced Gaseous tracking device Experiment) [22]. We developed a $\mu$-TPC with a detection volume of $23 \times 28 \times 30$ $cm^3$ and performed a direction-sensitive WIMP-search experiment in a surface laboratory.

* Corresponding author.
*E-mail address:* miuchi@cr.scphys.kyoto-u.ac.jp (K. Miuchi).

0370-2693 
doi:10.1016/j.physletb.2007.08.042

## 2. Detector performance

In this section, we describe the detector performance, which is also described in Ref. [23]. We mainly measured the detector response in the energy range that we used for the WIMP-search analysis (100–400 keV, DM energy range). The lower threshold (100 keV) was set at the lowest energy for an effective gamma-ray rejection with a 150 Torr $CF_4$ gas, and the higher threshold (400 keV) was set at the expected highest recoil energy by the WIMPs at the escape velocity.

### 2.1. $\mu$-TPC

A $\mu$-TPC is a gaseous time projection chamber with a micro pixel chamber ($\mu$-PIC) readout. A $\mu$-PIC is a gaseous two-dimensional position-sensitive detector manufactured by printed circuit board (PCB) technology. PCB technology realizes an economical mass production, which is one of the most important requirements to fabricate a dark matter detector. After a general-purposed detector R&D, we studied the performance of a $\mu$-TPC with a detection volume of $10 \times 10 \times 10$ cm$^3$ using a 150 Torr $CF_4$ gas as our first step towards a dark matter experiment [24]. In this study, we demonstrated the tracking of nuclear recoils and the gamma-ray rejection with a $CF_4$ gas of 150 Torr. We also found that we need some more studies to operate the $\mu$-TPC with a $CF_4$ gas at a design value of 30 Torr for more than a few days. We then developed a large-sized ($31 \times 31$ cm$^2$) $\mu$-PICs [25], and subsequently developed a large-volume $\mu$-TPC with a detection volume of $23 \times 28 \times 30$ cm$^3$. We studied the fundamental properties of this large-volume $\mu$-TPC with a standard Ar–$C_2H_6$ gas mixture at normal pressure [26]. The size is of the $\mu$-PIC is restricted by the working size of the PCB, and we plan to realize a larger readout area by placing many pieces, for instance $4 \times 4$ pieces for a 1 m$^2$, of $\mu$-PICs. Before we take the next technology steps, we performed a first direction-sensitive spin-dependent dark matter search experiment to demonstrate that a gaseous detector and a direction-sensitive method can actually set limits on the WIMPs. We report on the results of a direction-sensitive dark matter search experiment using this large-volume $\mu$-TPC with a 150 Torr $CF_4$ gas (9.0 g effective mass) in a surface laboratory.

We used the $\mu$-TPC described in Ref. [26], and thus most parts of the detector were unchanged. Herein, we describe only the significant properties and the modified parts of the detector system. Fig. 1 is a schematic drawing of the $\mu$-TPC. A $\mu$-PIC with a detection area of $31 \times 31$ cm$^2$ (TOSHIBA/DNP, SN060222-3) was used as the main gas-multiplier and as readout electrodes. A gas electron multiplier (GEM [27]) with an effective area of $23 \times 28$ cm$^2$, which was manufactured by a Japanese company (Scienergy Co. Ltd.), was used as a pre-amplifier. The drift length was 31 cm and the detection volume was $23 \times 28 \times 31$ cm$^3$. The electric field of the drift volume was formed with a field-shaping pattern on a fluorocarbon circuit board surrounding the detection volume. The detector was placed in a 3 mm-thick stainless-steel vacuum chamber filled with 150 Torr $CF_4$. The data-acquisition system, which is described in Ref. [28], was triggered by the signals of the

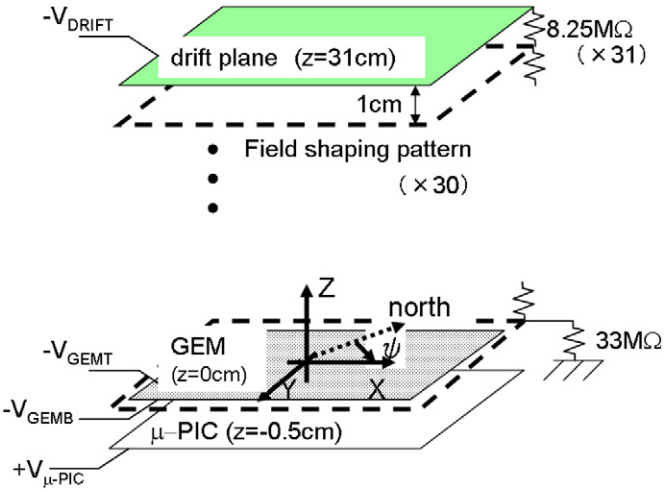


Fig. 1. Schematic drawings of the $\mu$-TPC. $\mu$-PIC and the GEM are set horizontally.

$\mu$-TPC itself. Hence, the absolute $Z$ position was not measured, but only the relative positions. Typical operation parameters were $V_{\mu\text{-PIC}} = 490$ V, $V_{\text{GEMB}} = 630$ V, $V_{\text{GEMT}} = 915$ V, and $V_{\text{DRIFT}} = 8.25$ kV. $V_{\mu\text{-PIC}}$ is the voltage supplied to the $\mu$-PIC, $V_{\text{GEMT}}$ is the voltage supplied to the top of the GEM, $V_{\text{GEMB}}$ is the voltage supplied to the bottom of the GEM, and $V_{\text{DRIFT}}$ is the voltage supplied to the drift plane. These parameters were optimized to realize stable operation at a combined ($\mu$-PIC × GEM) gas gain of 2300, which is high enough to maintain the detection efficiency of the recoil nucleus. We still suffer from discharge problems when operating a $\mu$-PIC alone.

### 2.2. Energy calibration and energy resolution

We calibrated and monitored the energy with alpha particles generated by the $^{10}\text{B}(n,\alpha)\,^7\text{Li}$ ($Q = 2.7$ MeV) reaction [23]. We set a glass plate coated with a thin 0.6 μm $^{10}$B layer in the $\mu$-TPC, and irradiated the $\mu$-TPC with thermalized neutrons. Alpha particles (5.6, 6.1, and 7.2 MeV) from the decays of the radon progeny were also used. The track-length and the energy-deposition correlation down to the DM energy range agreed with a calculation by SRIM [29].

The measured energy resolution in 5–8 MeV was 50% (FWHM), which was dominated by the gain inhomogeneity of the $\mu$-PIC. This would be the worst value when the gain inhomogeneity of the $\mu$-PIC dominates the energy resolution. The energy resolution could be dominated by the statistics of the primary electrons. In this case, the energy resolution at 100 keV with a $CF_4$ gas was estimated from a measurement with an Ar–$C_2H_6$ gas mixture, because it is not very easily measured due to a small photo-absorption cross-section and a long range of the electron. The energy resolution at 60 keV, measured with an Ar–$C_2H_6$ gas mixture, was 60% (FWHM) [26]. We calculated with $\Delta E_{\text{CF}_4} = \Delta E_{\text{Ar}} \cdot (\frac{60/W_{\text{Ar}}}{100/W_{\text{CF}_4}})^{1/2}$. Here, $\Delta E_{\text{CF}_4}$ and $\Delta E_{\text{Ar}}$ are the energy resolution at 100 keV with a $CF_4$ gas and that at 60 keV with an Ar–$C_2H_6$ gas mixture, respectively. $W_{\text{CF}_4} = 54$ eV and $W_{\text{Ar}} = 26$ eV are the energies needed to created an ion-electron pair in a $CF_4$ gas and an Ar–$C_2H_6$

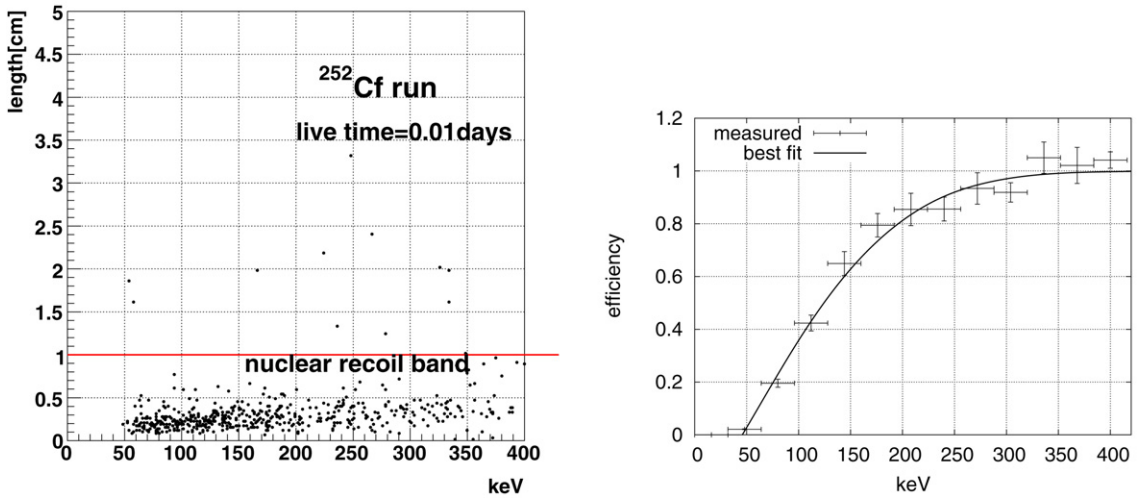


Fig. 2. Measured track-length and energy-deposition correlations with a neutron source of $^{252}$Cf (left) and the detection efficiency dependence on the recoil energy (right).

gas mixture, respectively. Thus, the estimated energy resolution was 70% (FWHM) at 100 keV with a $CF_4$ gas, if the statistics of the primary electron dominates the energy resolution. The energy resolution in the DM energy range was therefore estimated to be better than 70%.

### 2.3. Nuclear recoil detection efficiency

The nuclear-recoil detection efficiency was measured by irradiating the $\mu$-TPC with fast neutrons from a $^{252}$Cf source of 0.72 MBq placed at several positions. We selected the tracks within the fiducial volume ($21.5 \times 22 \times 31$ cm$^3$). We also required at least three digital hit points for a track. A typical track-length and energy-deposition correlation is shown in the left panel of Fig. 2. A nuclear recoil band is seen along the X-axis. We set the upper limit of the "nuclear recoil band" at 1 cm. We compared the spectrum after the selection with a simulated one, and the calculated ratio was the overall (detection and the selection) efficiency. The efficiency curve is shown in the right panel of Fig. 2. The efficiency was about 40% at 100 keV, and the efficiency dependence on the recoil energy was phenomenologicaly fitted with an error function, $\epsilon$. The best-fit function was $\epsilon = 1.0 \cdot \mathrm{erf}((E - 45.8)/165.2)$, where $\mathrm{erf}(x) = \frac{2}{\sqrt{\pi}} \int_0^x \exp(-x^2)\,dx$ is the error function and $E$ is the energy in keV.

### 2.4. Gamma-ray rejection factor

We demonstrated that the track-length and the energy-deposition correlation measured with a gaseous TPC provided a strong gamma-ray rejection in our previous work [24]. We performed quantitive measurements with a large-volume $\mu$-TPC for a WIMP-search measurement in a surface laboratory. We irradiated the $\mu$-TPC with gamma-rays from a $^{137}$Cs source of 0.80 MBq, placed at 25 cm from the center of the detection volume. The measured track-length and energy-deposition correlations with and without the gamma-ray source are shown in the left and the right panels of Fig. 3, respectively. The live time was 0.44 days for both measurements. A band along the Y-axis labeled "electron recoil band" is seen only in the results with a gamma-ray source, which is obviously due to tracks of the recoil electrons. Another band along the X-axis, seen in both results, is due to the tracks of the carbon and fluorine nuclei by the neutron background, and are labeled "nuclear recoil band". The spectra of these two measurements are shown in the left panel of Fig. 4. The spectrum of the no-source run was subtracted from the that of the $^{137}$Cs run. The obtained "subtracted" spectrum is shown in the right panel of Fig. 4. The subtracted spectrum is consistent with zero in the DM energy range, within the statistical error. We then derived the gamma-ray rejection factor by dividing the subtracted spectrum by a simulated electron recoil spectrum. The measured gamma-ray rejection factor in the DM energy range was $(0.57 \pm 0.69) \times 10^{-4}$. The error is statistical, which is dominated by the background in the surface laboratory. The 90% C.L. upper limit of the gamma-ray rejection factor was $1.5 \times 10^{-4}$.

### 2.5. Direction-dependent detection efficiency

The $\mu$-PIC has an anisotropic response with regard to the three-dimensional track directions. This non-uniform response is due to a difference in the detection method of the Z-axis (time information) and the other two axes (2-dimensional image taken by the $\mu$-PIC). We measured this detection efficiency dependence on the track direction, or a "response map", by irradiating the $\mu$-TPC with fast neutrons from several positions that generated uniform recoils. We fitted the digital hit points with a straight line, and determined the directions of each nuclear recoil track. Because we did not measure the track senses in this measurement, we fixed the sign of the x component to positive and determined the (x,y,z) vector of the track in the coordinates shown in Fig. 1. The measured response map is shown in Fig 5. The map was normalized by a mean value. It can be seen that the correction factor is quite large because the fabrication technology of the large-sized $\mu$-PIC is still in an R&D phase, and the gain inhomogeniety is still large. The detector showed a rel-

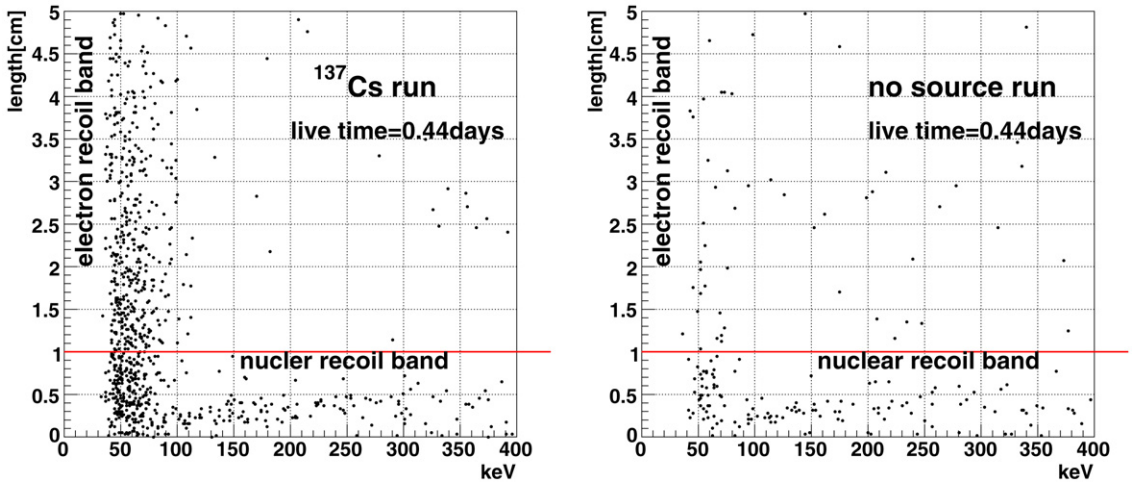


Fig. 3. Measured track-length and energy-deposition correlations with (left) and without (right) the gamma-ray source of $^{137}$Cs. Two bands along the Y- and X-axises are seen in the $^{137}$Cs run, while the electron recoil band is not seen in the no-source run. Several events out of both bands are thought to be the tracks of protons from the wall of the drift volume.

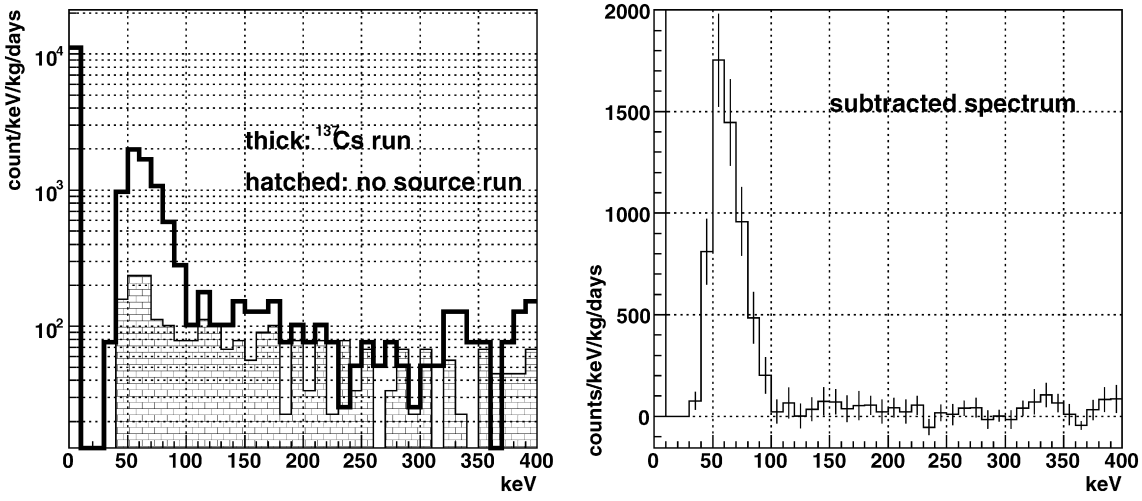


Fig. 4. Spectra taken with (thick) and without (hatched) the gamma-ray source of $^{137}$Cs (left) and the subtracted spectrum (right).

atively high efficiency for tracks in the X–Z and Y–Z planes, but showed a relatively low efficiency for tracks in the X–Y plane.

We have not overcome intrinsic weak points of the TPC that the efficiency to the tracks parallel to the readout plane is relatively low. It should be noted that the absolute detection efficiency was measured by a method described in the previous sections, and this response map was used to correct the relative efficiency.

### *2.6. Position resolution and angular resolution*

We measured the position resolution using the tracks of the alpha particles measured in the energy calibration. We evaluated the position resolution using the same method as described in our previous work [26]. The measured position resolution was 0.8 mm (rms). The angular resolution of the carbon and fluorine nuclei in the DM energy range was estimated in the following manner. We calculated the sampling pitch of the carbon and fluorine tracks from real data. We then generated the hit points by a simulation based on the measured position resolution and the sampling pitch. Simulated hit points were fitted with a straight line, and the angle between the fitted line and the real direction was calculated. The distribution of the calculated angle was fitted with a Lorentzian and $\gamma = 25°$, where $\gamma$ is a parameter of a Lorentzian that corresponds to HWHM. We used this value for a direction-sensitive analysis.

## 3. Measurement

A dark matter search measurement was performed in a surface laboratory at Kyoto University (Lat. 35°2′ N, Long. 135°47′ E, third floor in a five-story building). The measurement was performed from November 1st, 2006 to November 27th, 2006. We set the $\mu$-PIC plane horizontally and re-aligned the X- and Y-axis of the $\mu$-TPC twice (three different $\phi$ indicated in Fig. 1) so as to cancel any remaining static errors. Table 1 lists the measurement properties. The total live time was 16.71 days and the exposure was 0.151 kg days. The sum

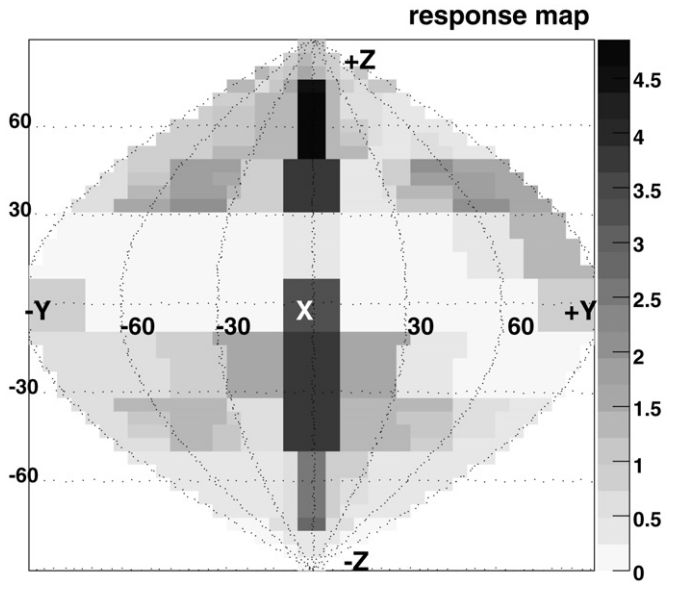


Fig. 5. Measured direction-dependent efficiency of the $\mu$-TPC. X means the direction along the X-axis. The map is normalized by the mean efficiency.

Table 1
Properties of the dark matter measurements

| X direction($\psi$) | Source | Live time [days] |
|---|---|---|
| $-5°$ | – | 4.37 |
| $40°$ | – | 5.25 |
| $18°$ | – | 4.95 |
| $18°$ | $^{137}$Cs | 2.14 |

of the calibration and maintenance time was 7.51 days, and the dead time due to the data acquisition was 1.0 days.

The $\mu$-TPC was filled with 150 Torr $CF_4$, and the vacuum chamber was sealed without any gas circulation. The drift velocity, total gas gain, and the energy resolution were monitored every two or three days during the measurement. The drift velocity was 7.6 cm/μs at the beginning of the measurement and decreased to 6.9 cm/μs at the end. This decrease is thought to be due to the out-gas from the detector components. We used the measured velocities for the analysis. The mean gas gain in the entire detection area was 2300, and a time-dependent variation was not observed within a measurement error of 4% (rms). The energy resolution was also stable within a measurement error of 7% (rms). The time-dependence was small compared to the energy resolution, itself, and the angular resolution in this measurement.

## 4. Results

The spectra did not show a statistically significant difference among the four conditions due to the strong gamma-ray rejection. We therefore combined the spectra obtained in the four measurements, including even the spectrum obtained in the gamma-ray rejection measurement with a $^{137}$Cs source. Fig. 6 shows the obtained spectrum in the DM energy range. The spectrum can be explained by a typical neutron flux in a surface laboratory of $O(1 \times 10^{-2}\,\mathrm{n\,cm^{-2}\,s^{-1}})$. We initially derived the

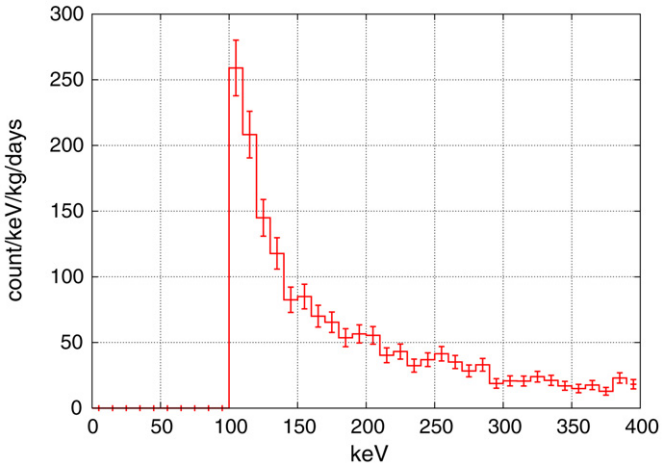


Fig. 6. Measured energy spectrum. The detection efficiency is taken into account.

Table 2
Astrophysical and nuclear parameters used to derive the WIMP-proton limits

| WIMP velocity distribution | Maxwellian |
|---|---|
| Solar velocity | $v_s = 244\,\mathrm{km\,s^{-1}}$ |
| Maxwellian velocity dispersion | $v_0 = 220\,\mathrm{km\,s^{-1}}$ |
| Escape velocity | $v_{esc} = 650\,\mathrm{km\,s^{-1}}$ |
| Local halo density | $0.3\,\mathrm{GeV\,cm^{-3}}$ |
| Spin factor of $^{19}$F | $\lambda^2 J(J+1) = 0.647$ |

limits of the WIMP-proton spin-dependent cross section only from the spectrum (conventional method). We used the parameters given in Table 2, and followed Ref. [30] for the calculation. The thin-dotted line, which is indicated by "spectrum only", in Fig. 9 shows the exclusion limits.

We next performed a direction-sensitive analysis. We created a sky map of the north sky with the direction of the three-dimensional nuclear recoil tracks. Because we did not detect the sense of each track, the map was restricted to half of the sky larger and the southern part of the sky was folded. We plotted every nuclear event (1686 events in a 0.151 kg days exposure) in Fig. 7. The larger mark, labeled "DM expected", is the direction of the solar motion or the Cygnus from which the WIMP-wind is expected. The WIMP-wind direction has a diurnal motion around the polestar. We calculated $\theta$, the angle between the WIMP-wind direction and the recoil direction for each event, and drew the $\cos\theta$ distribution shown in Fig. 8. We compared this measured $\cos\theta$ distribution with the expected WIMP-signal. The expected WIMP-signal was prepared by the following method. We first created a $\cos\theta$ distribution for a given WIMP mass and a recoil energy while considering the energy resolution. The DM energy range was divided into 15 bins, and the energy and angular resolution of the detector were taken into account. We used 70% (FWHM) for the energy resolution and an angular resolution of $\gamma = 25°$. We followed Ref. [16] for the angular distribution and Ref. [30] for the count rate. We then created a sky-map expected by the WIMP events with this $\cos\theta$ distribution while considering the direction-dependence (Fig. 5) and the angular resolution. We used this sky map to cre-

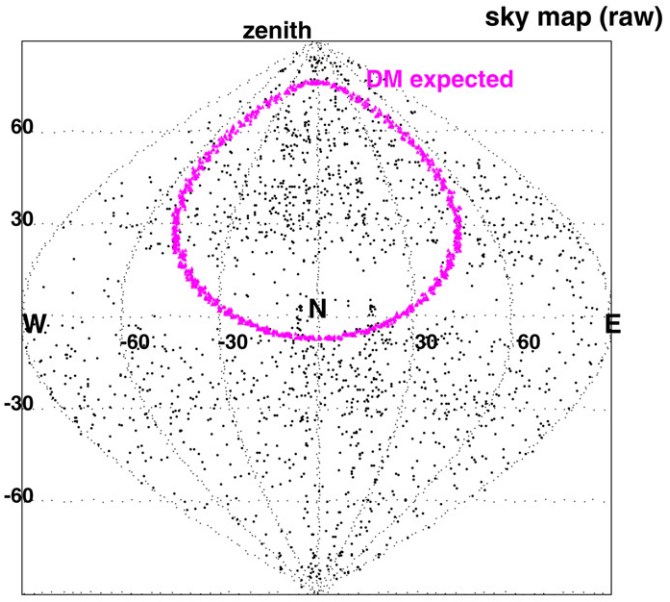


Fig. 7. Obtained sky map of the north sky. The recoil directions of the fluorine and carbon nuclei are used. A raw map and a corrected map by the relative efficiency dependent on the directions are shown. The thick line indicates the direction of the solar motion (direction of the WIMP-wind).

ate the expected $\cos\theta$ distribution for a given WIMP mass and energy bin. Fig. 8 shows one of these $\cos\theta$ distributions. Here, the data was fitted with the distribution for $M_\chi = 100$ GeV and 100–120 keV bin, and the cross section that gave the minimum $\chi^2$ was $1.36 \times 10^4$ pb and $\chi^2/\text{d.o.f.} = 22.4/9$. This best-fitted WIMP signal was rejected at the 90% confidence level by $\chi^2$ tests. The cross section that would give the minimum $\chi^2$ was calculated for each energy bin, and the smallest cross section was taken as the limit for the given WIMP mass. The upper and lower panels in Fig. 9 show the cross section limits and the corresponding $\chi^2$ values as a function of the WIMP mass, respectively. The limits are shown with a thick-solid line (labeled "direction-sensitive") and the $\chi^2$ values are shown by filled-square marks. The $\chi^2$ values at the 90% C.L. upper limit are shown by a dotted line in the lower panel in Fig. 9. The WIMP signals were rejected at the 90% confidence level because the best-fit $\chi^2$ values were all above the 90%-$\chi^2$ line. The data was also fitted with a flat $\cos\theta$ distribution and $\chi^2/\text{d.o.f.} = 9.9/9$ was obtained independent of the WIMP mass. The flat $\cos\theta$ was not rejected at the 90% confidence level. It was demonstrated that the direction-sensitive method gave a limit slightly better than the conventional spectrum-only method. The difference between this result and other experiments is explained by the neutron background in the surface laboratory. This is the first limit set by a dark matter search experiment with a gaseous tracking device. As for the spin-dependent limit, this is the first result by a direction-sensitive experiment. It should be stressed that the dark matter search experiment with a gaseous tracking device can actually set a limit on the WIMPs. These results are very convincing and encouraging towards developing a future WIMP-wind detection with large-volume detectors.

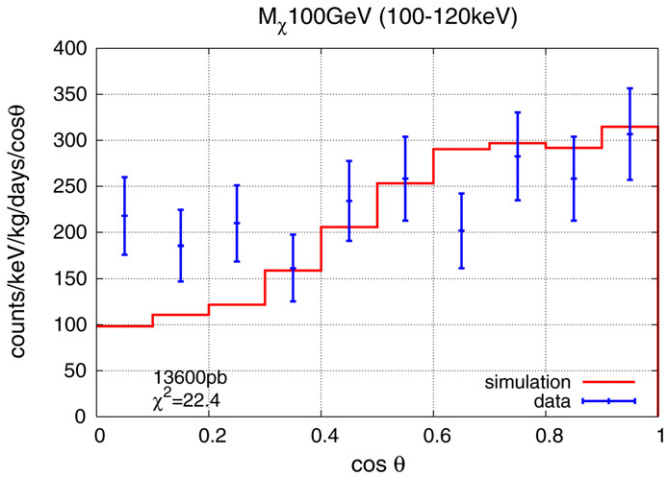


Fig. 8. Measured (with error bars) and expected (histogram) distribution of the angle between the recoil direction and the WIMP direction. The expected histogram is that with $M_\chi = 100$ GeV, 100–120 keV bin, and $1.36 \times 10^4$ pb.

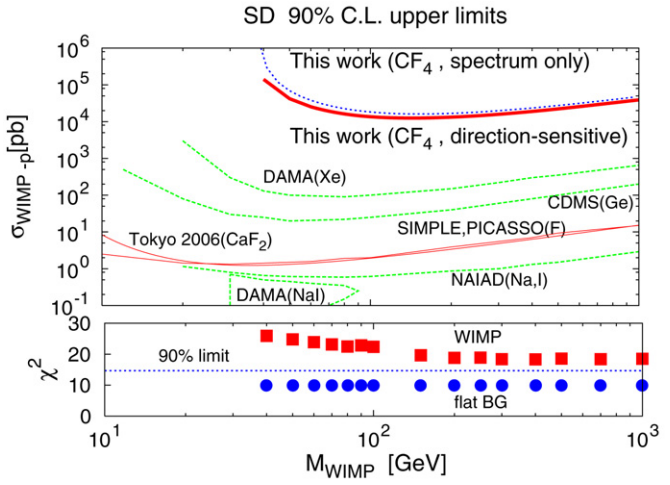


Fig. 9. 90% C.L. upper limits on the WIMP-proton spin-dependent cross section (upper) and $\chi^2$ values (lower) as functions of the WIMP mass. The thick solid and dotted lines show the limits obtained with and without the direction information, respectively. Limits from other experiments (DAMA(Xe) [3], DAMA(NaI) [4], NAIAD [5], Tokyo $CaF_2$ [7], SIMPLE 2005 [10], PICASSO [11], and CDMS [12]) are shown for comparison. The filled squares show the $\chi^2$ minimum values of the best-fit WIMP distribution, the filled-circles show the best-fit flat $\cos\theta$ distribution, and the dotted line show the $\chi^2$ values at the 90% C.L. upper limit.

## 5. Discussions

We have shown that WIMP-proton cross section limits can be obtained by a direction-sensitive method. However, much work is necessary to reach the sensitivity achieved by other experiments performed with solid and liquid detectors. The sensitivity is restricted by the neutron background in a surface run, therefore, we are going to perform a dark matter search experiment in an underground laboratory. The fast neutron flux in Kamioka Observatory ($(1.9 \pm 0.21) \times 10^{-6}\,\text{n}\,\text{cm}^{-2}\,\text{s}^{-1}$) is more than 3 orders of magnitude smaller than a typical fast neutron flux in a surface laboratory. It expected that the background sources, such as radioactive isotopes in the detector compo-

nents, would limit the sensitivity in the first stage of an underground run. We are going to replace the detector components with low-activity materials. The angular resolution is not good enough to take full advantage of the direction-sensitive method over the "spectrum only" method. We are going to investigate the detector response using a neutron source of a known energy. We plan to study the operation of the $\mu$-TPC at a lower pressure of 30 Torr to lower the energy threshold. We are going to develop a larger readout area by placing many pieces of the of $\mu$-PICs of $31 \times 31$ cm$^2$. After these technological breakthroughs are achieved, we expect to reach the SUSY predictions with an exposure of more than one hundred kg days, which we have calculated in our previous work [22].

## 6. Conclusion

We developed a three-dimensional tracking device, and performed a direction-sensitive dark matter search measurement in a surface laboratory. By using 150 Torr carbon-tetrafluoride ($CF_4$) gas, we set the first limit on the spin-dependent WIMP-proton cross section by a direction-sensitive method. Thus, we have demonstrated that a dark matter search experiment with a gaseous tracking device can actually set a limit on WIMPs. Furthermore, we have demonstrated that this method will potentially play a certain role in revealing the nature of dark matter when a low-background large-volume detector is developed.

## Acknowledgements

This work was supported by a Grant-in-Aid in Scientific Research of the Ministry of Education, Culture, Sports, Science, Technology of Japan; research-aid program of Toray Science Foundation; and Grant-in-Aid for the 21st Century COE "Center for Diversity and Universality in Physics".

## References

[1] D.N. Spergel, et al., Astrophys. J. Suppl. 148 (2003) 175;
D.N. Spergel, et al., astro-ph/0603449.
[2] P. Belli, R. Bernabei, A. Incicchitti, D. Prosperi, Nuovo Cimento C 15 (1992) 475;
R. Bernabei, P. Belli, F. Nozzoli, A. Incicchitti, Eur. Phys. J. C 28 (2003) 203.
[3] R. Bernabei, et al., Phys. Lett. B 436 (1998) 379.
[4] R. Bernabei, et al., Phys. Lett. B 424 (1998) 195;
R. Bernabei, et al., Phys. Lett. B 450 (1999) 448;
R. Bernabei, et al., Phys. Lett. B 480 (2000) 23;
R. Bernabei, et al., astro-ph/0307403.
[5] B. Ahmed, et al., Astropart. Phys. 19 (2003) 691.
[6] H. Sekiya, et al., in: N.J.C. Spooner, V. Kudryavtsev (Eds.), Proceedings of the Fourth International Workshop on "The Identification of Dark Matter", Edinburgh, UK, 2004, World Scientific, 2005, p. 378.
[7] Y. Shimizu, et al., Phys. Lett. B 633 (2006) 195.
[8] G. Angloher, et al., Astropart. Phys. 23 (2005) 325.
[9] G.J. Alner, et al., Astropart. Phys. 23 (2005) 444.
[10] T.A. Girard, et al., Phys. Lett. B 621 (2005) 233.
[11] M. Barnabé-Heider, et al., Phys. Lett. B 624 (2005) 186.
[12] CDMS Collaboration, Phys. Rev. D 72 (2005) 052009.
[13] EDELWEISS Collaboration, Phys. Rev. D 71 (2005) 122002.
[14] G.J. Alner, et al., Nucl. Instrum. Methods A 555 (2005) 173.
[15] R.W. Schenee, et al., astro-ph/0502435.
[16] D.N. Spergel, Phys. Rev. D 37 (1988) 1353.
[17] A.M. Green, B. Morgan, Astropart. Phys. 27 (2007) 142.
[18] J. Rich and M. Spiro, Saclay preprint DPhPE 88-04 (1988);
G. Gerbier, J. Rich, M. Spiro, C. Tao, in: E.B. Norman (Ed.), Proceedings of the Workshop on "Particle Astrophysics", World Scientific, 1989, p. 43.
[19] G. Masek, K. Buckland, M. Mojaver, in: E.B. Norman (Ed.), Proceedings of the Workshop on "Particle Astrophysics", World Scientific, 1989, p. 41.
[20] J.I. Collor, et al., New J. Phys. 2 (2000) 14.1.
[21] T.A. Girard, F. Giuliani, Phys. Rev. D 75 (2007) 043512.
[22] T. Tanimori, et al., Phys. Lett. B 578 (2004) 241.
[23] K. Miuchi, et al., physics/0701118.
[24] H. Sekiya, et al., Nucl. Instrum. Methods A 573 (2007) 204.
[25] A. Takada, et al., Nucl. Instrum. Methods A 573 (2007) 195.
[26] K. Miuchi, et al., Nucl. Instrum. Methods A 576 (2007) 43.
[27] F. Sauli, A. Sharma, Annu. Rev. Nucl. Part. Sci. 49 (1999) 341.
[28] H. Kubo, et al., IEEE Nuclear Science Symposium Conference Record N14-30 (2005).
[29] J.F. Ziegler, J.P. Biersack, U. Littmark, SRIM—The Stopping and Range of Ions in Matter, Pergamon Press, New York, 1985.
[30] J.D. Lewin, P.F. Smith, Astropart. Phys. 6 (1996) 87.